Coexistence of charge-2 Dirac and Weyl phonons in chiral space groups

Guang Liu,[1] Zhenqiao Huang,[1,2] Zhongjia Chen,[1,3] Yuanjun Jin,[1,4] Changchun He,[1,5] and Hu Xu[1,6,7,*]

[1]*Department of Physics, Southern University of Science and Technology, Shenzhen 518055, People's Republic of China*
[2]*Department of Physics, The Hong Kong University of Science and Technology, Clear Water Bay, Hong Kong 999077, People's Republic of China*
[3]*Songshan Lake Materials Laboratory, Dongguan, Guangdong 523808, People's Republic of China*
[4]*Division of Physics and Applied Physics, School of Physical and Mathematical Sciences, Nanyang Technological University, 637371 Singapore*
[5]*Department of Physics, South China University of Technology, Guangzhou 510640, Peoples Republic of China*
[6]*Shenzhen Key Laboratory of Advanced Quantum Functional Materials and Devices, Southern University of Science and Technology, Shenzhen 518055, People's Republic of China*
[7]*Guangdong Provincial Key Laboratory of Computational Science and Material Design, Southern University of Science and Technology, Shenzhen 518055, Peoples Republic of China*

(Received 27 April 2022; accepted 4 August 2022; published 12 August 2022)

Unconventional topological phonons with unusual properties in crystalline solids have attracted increasing attention. By performing symmetry arguments and low-energy effective Hamiltonian, we confirm the coexistence of charge-2 Dirac and Weyl phonons at high-symmetry points and high-symmetry lines by analyzing all possible space groups. We reveal that such a particular system only emerges in chiral space groups in the presence of time-reversal symmetry. Unlike conventional Weyl pairs with opposite chirality that host one surface arc, there are two surface arcs by connecting one charge-2 Dirac point with topological charge $= \pm 2$ and two Weyl points with topological charge $= \mp 1$. Due to the constraints of symmetry arguments and projection direction in chiral crystals, the surface arcs are long enough to span over the whole surface Brillouin zone. We take $Na_2Zn_2O_3$ as an example to confirm our predication, and two branches of surface states across the whole surface Brillouin zone are clearly visible. Our work not only presents exotic quasiparticles but also provides an idea for realizing long nontrivial surface arcs.

DOI: 10.1103/PhysRevB.106.054306

I. INTRODUCTION

Since the discovery of topological insulators [1,2], various topological phases of matter (e.g., topological crystalline insulators [3–5], topological superconductors [6–8], higher-order topological insulators [9,10], and topological semimetals [11–13]) based on symmetry and topology have been theoretically predicted and experimentally confirmed, enriching the topological classification. In particular, topological semimetals including Dirac semimetals [12–16], Weyl semimetals [11,17–19], and nodal-line semimetals [20–22] have attracted much research attention owing to their intriguing properties.

Weyl points (WPs) are characterized by an isolated point touching of two bands in momentum space, which act as "source" or "sink" of Berry curvature. Therefore, the topology of WPs can be defined by a quantized chiral charge, which is the flux of the Berry curvature passing through a closed surface in momentum space [23,24]. As the fourfold degenerate Dirac points (DPs) characterized by zero topological charge can be regarded as the overlap of two WPs with opposite chiral charges, WPs can be realized by breaking either the time-reversal ($\mathcal{T}$) symmetry or inversion ($\mathcal{P}$) symmetry in Dirac semimetals [14,15,25–27]. In addition to the conventional DPs, there are unconventional DPs in chiral crystals. Since the inversion and mirror symmetries are broken in chiral crystals, the topological charge of a fourfold degenerate point is +2 or –2 in chiral space groups, which is usually called a charge-2 Dirac point (CDP) [28–30]. Although the Nielsen-Ninomiya no-go theorem [31,32] is still preserved in chiral crystals, topological quasiparticles with opposite chirality do not coincide in energy, probably leading to the formation of unpaired chiral quasiparticles [33–35].

Phonons are bosons, which are not limited by the Pauli exclusion principle. Therefore, all phonons in crystalline solids can be excited and their topological features in the whole frequency range can also be physically observed. In recent years, the concept of topology (e.g., Berry phase, Berry curvature, or topological charge) has been extended to phonon systems, giving rise to distinct types of topological phonons [28–30,33–51], which includes Weyl phonons [33–40], Dirac phonons [41–43], triple point phonons [44], nodal-line phonons [45–47], and nodal-surface phonons [48,49]. In particular, the coexistence of topological phonons in realistic materials has attracted much attention, such as the coexistence of zero-, one-, and two-dimensional degeneracy phonons [52], hybrid-type nodal-ring and quadratic nodal-line phonons [53],

*xuh@sustech.edu.cn

and nodal-net and nodal-link phonons [54]. However, the coexisting topological phonons mentioned above only occasionally emerge in a system due to symmetry constraints in crystalline solids, indicating that there is no direct relationship between different types of topological phonons in the above systems. To deepen our understanding of interplay between topological phonons, it is highly desired to study the coexistence of different chiral topological phonons. So far, the coexistence of CDP with topological charge $= \pm 2$ and WPs with topological charge $= \mp 1$ has not been reported.

In this work, we perform symmetry analysis to find the possible coexistence of CDP and WPs at high-symmetry points and high-symmetry lines. Our results show that only chiral space groups 19, 90, 92, 94, and 96 possess such unconventional topological phonons. We reveal that CDPs originate not only from the essential degeneracy located at high-symmetry points but also from the accidental degeneracy along high-symmetry lines. More importantly, by combining the momentum position of phonons and the projection direction of surface states, we can design long surface arcs that span the whole surface Brillouin zone (BZ). Through high-throughput calculations and symmetry analysis, we propose many materials as attractive candidates to study the coexistence of CDP and WPs with fascinating topological surface arcs, providing an ideal platform to study the entanglement between CDP and WPs.

TABLE I. The possible coexistence of charge-2 Dirac and Weyl phonons at high-symmetry points and high-symmetry lines. The first column indicates the space group (SG) number. The second and fourth columns indicate the high-symmetry points and high-symmetry lines possessing one CDP and WPs, respectively. The third and fifth columns indicate the generators of the CDP and WP, respectively. Symmetry operations with wavy lines indicate nonsymmorphic operations.

SG	CDP	Generators	WP	Generators
19($P2_12_12_1$)	R	$\widetilde{C}_{2x}, \widetilde{C}_{2y}, \mathcal{T}$	Γ-X	$\widetilde{C}_{2x}$
			Γ-Y	$\widetilde{C}_{2y}$
			Γ-Z	$\widetilde{C}_{2z}$
90($P42_12$)	M-A	$\widetilde{C}_{4z}$	Γ-X	$\widetilde{C}_{2y}$
			Γ-M	C_{2xy}
			R-Z	$\widetilde{C}_{2y}$
			A-Z	C_{2xy}
92($P4_12_12$)	A	$\widetilde{C}_{4z}, \widetilde{C}_{2x}, \mathcal{T}$	Γ-Z	$\widetilde{C}_{4z}$
	M-A	$\widetilde{C}_{4z}$	Γ-X	$\widetilde{C}_{2y}$
			Γ-M	C_{2xy}
94($P4_22_12$)	M-A	$\widetilde{C}_{4z}$	Γ-X	$\widetilde{C}_{2y}$
			Γ-M	C_{2xy}
			R-Z	$\widetilde{C}_{2y}$
			A-Z	C_{2xy}
96($P4_32_12$)	A	$\widetilde{C}_{4z}, \widetilde{C}_{2x}, \mathcal{T}$	Γ-Z	$\widetilde{C}_{4z}$
	M-A	$\widetilde{C}_{4z}$	Γ-X	$\widetilde{C}_{2y}$
			Γ-M	C_{2xy}

II. RESULTS AND DISCUSSION

We take the space group 96 as an example to analyze the coexistence of CDP and WPs, and more results for other possibilities are provided in the Supplemental Material (SM) [55]. As listed in Table I, there is a CDP at the high-symmetry point A with momentum position $(\frac{1}{2}, \frac{1}{2}, \frac{1}{2})$ in space group 96. The symmetry at A is characterized by three generators: $\widetilde{C}_{4z} \equiv \{C_{4z}|\frac{1}{2}\frac{1}{2}\frac{3}{4}\}$, $\widetilde{C}_{2x} \equiv \{C_{2x}|\frac{1}{2}\frac{1}{2}\frac{1}{4}\}$, and $\mathcal{T}$. By performing symmetry operations on the lattice, the space coordinates will be transformed from (x, y, z) to (x', y', z'), thus we can define the operators as

$$\begin{aligned} \widetilde{C}_{4z} &: (x, y, z) \to \left(-y + \tfrac{1}{2}, x + \tfrac{1}{2}, z + \tfrac{3}{4}\right), \\ \widetilde{C}_{2x} &: (x, y, z) \to \left(x + \tfrac{1}{2}, -y + \tfrac{1}{2}, -z + \tfrac{1}{4}\right). \end{aligned} \tag{1}$$

At A, we have the relation

$$\widetilde{C}_{4z}^4 = T_{003} = -1, \quad \widetilde{C}_{2x}^2 = T_{100} = -1, \tag{2}$$

and

$$\widetilde{C}_{4z}\widetilde{C}_{2x} = \widetilde{C}_{2x}\widetilde{C}_{4z}^3, \tag{3}$$

where T_r denotes the lattice translation along r. We take the eigenstates of $\widetilde{C}_{4z}$ as the Bloch states at A, which are denoted as $|c_{4z}\rangle$ with $c_{4z} \in \{\pm e^{i\pi/4}, \pm e^{-i\pi/4}\}$. By using commutation relations of symmetry operations, we can construct four linearly independent states $\{|e^{i\pi/4}\rangle, \mathcal{T}|e^{i\pi/4}\rangle, \mathcal{T}\widetilde{C}_{2x}|e^{i\pi/4}\rangle, \widetilde{C}_{2x}|e^{i\pi/4}\rangle\}$. It is easy to prove that they form a fourfold degenerate CDP. The matrix representations of symmetry operations can be expressed by the above basis as

$$\begin{aligned} D(\widetilde{C}_{4z}) &= \sigma_z \otimes e^{i\tau_z\pi/4}, \\ D(\widetilde{C}_{2x}) &= -i\sigma_y \otimes \tau_x, \\ D(\mathcal{T}) &= \sigma_o \otimes \tau_x\mathcal{K}, \end{aligned} \tag{4}$$

where $\sigma_{x,y,z}$ and $\tau_{x,y,z}$ are Pauli matrices, and $\mathcal{K}$ denotes the complex conjugation operator. According to the invariant theory, the Hamiltonian $\mathcal{H}_{\text{eff}}$ remains invariant under the symmetry transformations, namely,

$$\begin{aligned} D(\widetilde{C}_{4z})\mathcal{H}_{\text{eff}}(\mathbf{k})D^{-1}(\widetilde{C}_{4z}) &= \mathcal{H}_{\text{eff}}(-k_y, k_x, k_z), \\ D(\widetilde{C}_{2x})\mathcal{H}_{\text{eff}}(\mathbf{k})D^{-1}(\widetilde{C}_{2x}) &= \mathcal{H}_{\text{eff}}(k_x, -k_y, -k_z), \\ D(\mathcal{T})\mathcal{H}_{\text{eff}}(\mathbf{k})D^{-1}(\mathcal{T}) &= \mathcal{H}_{\text{eff}}(-k_x, -k_y, -k_z). \end{aligned} \tag{5}$$

Under the constraints in Eq. (5), the effective model can be written as

$$\mathcal{H}_{\text{eff}}(\mathbf{k}) = a_1k_x\Gamma_{y,x} - a_2k_y\Gamma_{y,y} + a_3k_z\Gamma_{0,z}, \tag{6}$$

where $a_{1,2,3}$ are real parameters and $\Gamma_{i,j} = \sigma_i \otimes \tau_j$. The Hamiltonian exhibits the fourfold degeneracy at $\mathbf{k} = 0$ and the linear dispersion when $\mathbf{k} \to 0$.

In space group 96, it is possible for a WP to locate at the high-symmetry line Γ-Z $(0, 0, w)$. The little group can be generated by the screw rotation symmetry $\widetilde{C}_{4z} \equiv \{C_{4z}|\frac{1}{2}\frac{1}{2}\frac{3}{4}\}$, which changes the coordinates of the lattice as

$$\widetilde{C}_{4z} : (x, y, z) \to (-y + \tfrac{1}{2}, x + \tfrac{1}{2}, z + \tfrac{3}{4}). \tag{7}$$

Then we can get the relation

$$\widetilde{C}_{4z}^4 = T_{003} = e^{6i\pi w}. \tag{8}$$

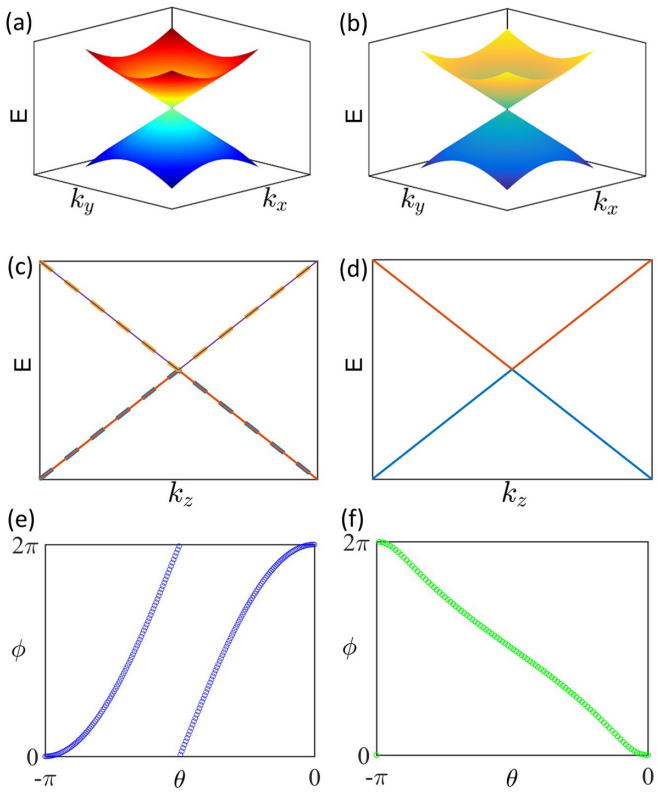

FIG. 1. Three-dimensional representation of phonon dispersions in the k_x-k_y plane by $\mathbf{k}\cdot\mathbf{p}$ model analysis for (a) a fourfold degenerate CDP and (b) a twofold degenerate WP. Phonon dispersions along the k_z axis for (c) a CDP and (d) a WP. The evolution of WCCs for (e) a CDP and (f) a WP.

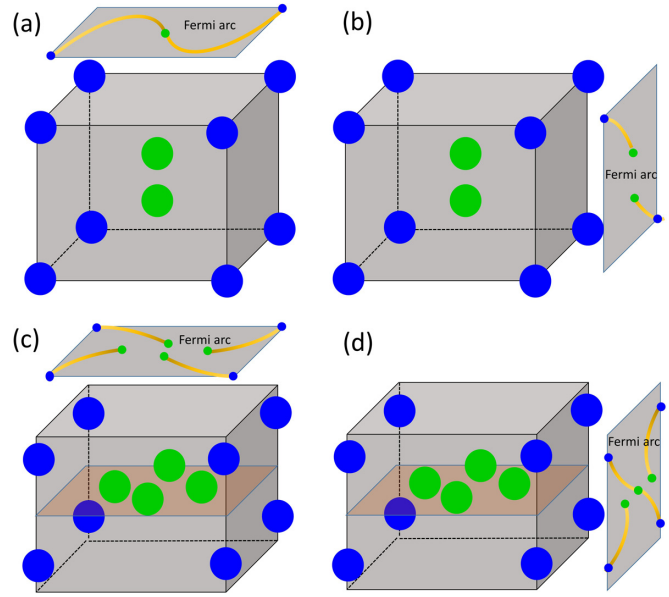

FIG. 2. Schematic diagrams of CDPs at high-symmetry points with (a) (001) and (b) (010) surface arcs. CDPs along high-symmetry lines with (c) (001) and (d) (010) surface arcs. The blue dots at the boundary of BZ represent CDPs, and the green dots inside the BZ represent WPs.

Hence, the eigenvalues of $\widetilde{C}_{4z}$ can be expressed as

$$E_n = \{e^{in\pi/2}e^{3i\pi w/2}, n = 0, 1, 2, 3\}, \tag{9}$$

which can be used to indicate each phonon branch. When two phonon branches with different eigenvalues cross on this $\widetilde{C}_{4z}$ invariant path, the matrix representation of $\widetilde{C}_{4z}$ can be written as

$$D(\widetilde{C}_{4z}) = e^{3i\pi w/2}\begin{pmatrix} e^{i\pi n_1/2} & \\ & e^{i\pi n_2/2} \end{pmatrix}. \tag{10}$$

When $e^{(n_1-n_2)i\pi/2} = \pm i$, there can exist a single WP, and the Hamiltonian can be expressed as

$$\mathcal{H}_{\text{eff}}(\mathbf{k}) = a_1\sigma_z k_z + \alpha_1\sigma_+(k_x \pm ik_y) + \text{H.c.}, \tag{11}$$

where a_1 is a real parameter, α_1 is a complex parameter, and $\sigma_\pm = \sigma_x \pm i\sigma_y$. The Hamiltonian exhibits the twofold degeneracy at $\mathbf{k} = 0$ and the linear dispersion when $\mathbf{k} \to 0$.

Using the $\mathbf{k}\cdot\mathbf{p}$ effective model Hamiltonian described above, we plot the three-dimensional representation of phonon dispersions in the k_x-k_y plane for a CDP and a WP in Figs. 1(a) and 1(b), respectively. Both the fourfold band degeneracy CDP and twofold band degeneracy WP possess linear dispersion along the k_z axis, as shown in Figs. 1(c) and 1(d), respectively. To determine the topological charges of these topological quasiparticles, we perform the Wilson loop approach to calculate the flux passing through a sphere enclosing a CDP or WP [56,57]. By examining the evolution of the Wannier charge centers (WCCs), we can visually determine the topological charges of these nodes. As shown in Figs. 1(e) and 1(f), the topological charges of a CDP and a WP are 2 and 1, respectively, which further confirms our model.

To elaborate the topological features in our model, we consider different combinations of CDPs (see blue dots) and WPs (see green dots) in Fig. 2. When CDPs are located at the high-symmetry points, the schematic diagrams of (001) and (010) surface arcs are shown in Figs. 2(a) and 2(b), respectively. It is clear that a long surface arc spans the entire (001) surface BZ. If CDPs appear at the high-symmetry lines, several long surface arcs are clearly visible in Figs. 2(c) and 2(d), and, among them, a long surface arc spanning the entire (010) surface BZ is also found.

Based on the above analysis, we perform first-principles calculations to confirm the existence of chiral topological phonons. The realistic $Na_2Zn_2O_3$ with space group $P4_32_12$ (No. 96) is taken as a candidate [58], and more candidates are provided in the SM [55]. The primitive cell of $Na_2Zn_2O_3$ contains eight Na, eight Zn, and twelve O atoms, as shown in Fig. 3(a). The optimized lattice constants are $a = 6.164$ Å and $c = 9.281$ Å, which are in good agreement with the experimental values [58]. The bulk BZ and the corresponding (010) and (001) surface BZs are shown in Fig. 3(b). As shown in Fig. 3(c), the phonon spectrum is plotted, and there is no imaginary frequency. In $Na_2Zn_2O_3$, the fourfold rotational symmetry and three twofold rotational symmetries perpendicular to each other give rise to a CDP. The CDP in $Na_2Zn_2O_3$ is contributed from the 81st to 84th phonon branches, which is located at the high-symmetry point A [see the blue dot in Fig. 3(b)]. The WPs are along the high-symmetry line Γ-Z.

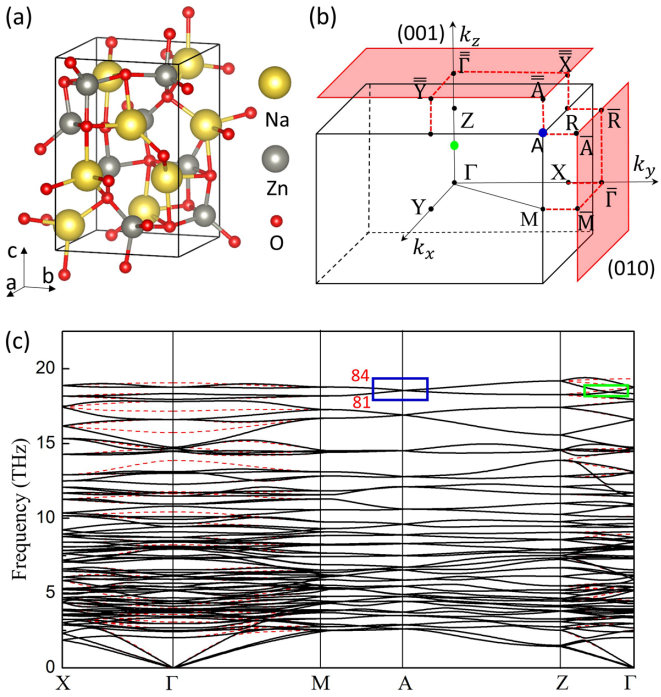

FIG. 3. (a) Primitive cell of $Na_2Zn_2O_3$ and (b) the corresponding bulk BZ and surface BZs. (c) Phonon spectrum of $Na_2Zn_2O_3$ along the high-symmetry lines with (red dashed lines) or without (black solid lines) non-analytic term correction. The blue and green boxes mark a fourfold degenerate CDP and a twofold degenerate WP, respectively.

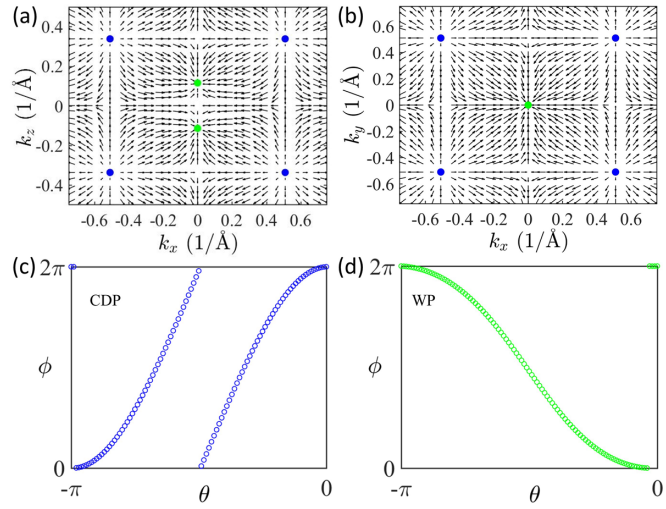

FIG. 4. Berry curvature of $Na_2Zn_2O_3$ in (a) the k_x-k_z and (b) k_x-k_y planes. The blue exceptional points denote CDPs, and green exceptional points denote WPs. The evolution of WCCs for (c) the CDP and (d) the WP.

The nonanalytic term correction to the dynamics matrix to deal with long-range interactions in $Na_2Zn_2O_3$ is applied, which does not change the topological features of $Na_2Zn_2O_3$. Therefore, $Na_2Zn_2O_3$ is a perfect platform to realize the coexistence of charge-2 Dirac and Weyl phonons.

As shown in Figs. 4(a) and 4(b), the distribution of Berry curvature in the k_x-k_z and k_x-k_y planes exhibits a nontrivial vortex feature in momentum space. To further confirm the topologically protected nodes, the Wilson loop approach is performed to calculate topological charges of CDPs and WPs. We find that $Na_2Zn_2O_3$ possesses one CDP with topological charge $= +2$ and two equal WPs with topological charge $= -1$, which is corresponding to our model analysis. As there exist one CDP and two WPs, it still satisfies the "no-go" theorem.

We next turn to examine surface states and surface arcs to explore unusual behaviors of the coexistence system. At first, the phonon local density of states (LDOS) projected on the (010) surface of $Na_2Zn_2O_3$ is plotted in Fig. 5(a), in which the surface states connect the WP [projected to the general point along $\bar{\Gamma}$-$\bar{R}$] and CDP [projected to $\bar{A}$] are clearly visible. We also plot the isofrequency surface contour of the (010) surface, as shown in Fig. 5(b). As expected, the surface arcs look similar to our analysis in Fig. 2(b). Constrained by topological chiral charges, the phonon surface arcs terminated at $\bar{A}$ [the corner in Fig. 5(b)] are shared by another WP in the neighboring BZ. In addition, the phonon surface states projected on the (001) surface are given in Fig. 5(c), which are terminated at the projection of the CDP [projected to $\bar{\bar{A}}$] and two WPs [projected to $\bar{\bar{\Gamma}}$]. We also plot the isofrequency surface contour of the (001) surface in Fig. 5(d). Similar to the case in Fig. 5(b), the phonon surface arcs terminated at $\bar{\bar{A}}$ [the corner in Fig. 5(d)] are shared by one WP at $\bar{\bar{\Gamma}}$ [the center in Fig. 5(d)] and another WP in the neighboring BZ, and these phonon surface states span over the whole surface BZ. As shown in Fig. 5(e), we choose five isofrequency surfaces, and the evolution of surface arcs projected on the (001) surface is clearly visible. Interestingly, a Lifshitz-like transition originated from the saddlelike dispersion in the k_x-k_y plane is found, and the critical isofrequency surface of the transition occurs at 18.628 THz.

III. CONCLUSIONS

In summary, we propose the coexistence of charge-2 Dirac and Weyl phonons by screening symmetry conditions in chiral space groups. Due to symmetry constraints, it is possible to design extremely long surface phonon arcs in chiral crystals. Using high-throughput calculations and symmetry analysis, we identify many materials as candidates with nontrivial phonon surface arcs. In addition, a Lifshitz-like transition originated from the saddlelike dispersion emerges in this coexistence system. Our work enriches the classification of topological phonons and provides an interesting platform to study the interplay between WPs and CDPs. Our results are also expected to extend to fermionic systems.

ACKNOWLEDGMENTS

This work is supported by the National Natural Science Foundation of China (No. 11974160), the Science, Technology, and Innovation Commission of Shenzhen Municipality (No. RCYX20200714114523069 and No. ZDSYS20190902092905285), the fund of the

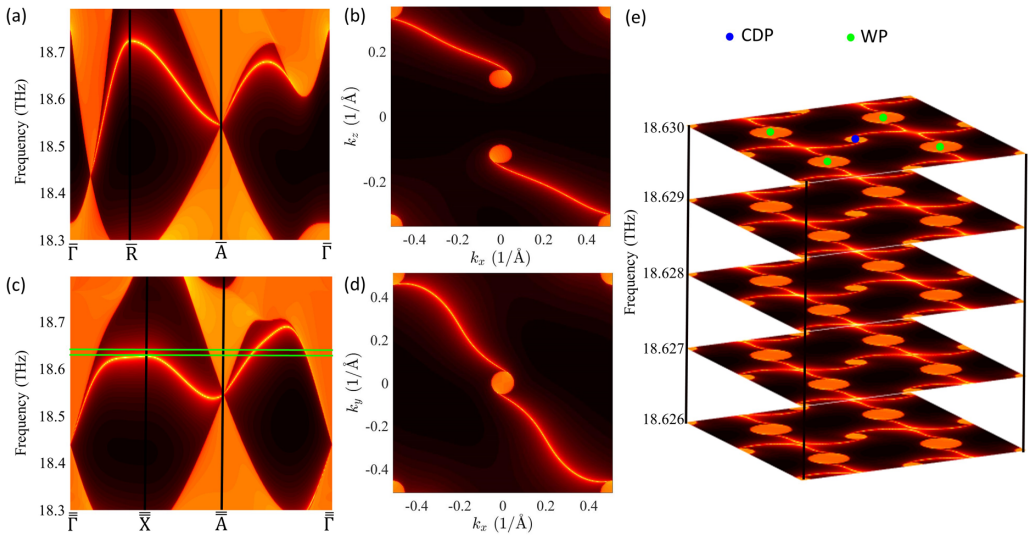

FIG. 5. LDOS projected on the semi-infinite (a) (010) and (c) (001) surfaces. The isofrequency surfaces at 18.5 THz projected on the (b) (010) and (d) (001) surfaces. (e) The isofrequency crosssections of (001) at five frequencies are indicated by two solid green lines in (c). The blue and green dots denote the projections of the CDP and WP, respectively.

Guangdong Provincial Key Laboratory of Computational Science and Material Design (No. 2019B030301001), and the Center for Computational Science and Engineering at Southern University of Science and Technology.

[1] M. Z. Hasan and C. L. Kane, Rev. Mod. Phys. **82**, 3045 (2010).
[2] X. L. Qi and S. C. Zhang, Rev. Mod. Phys. **83**, 1057 (2011).
[3] L. Fu, Phys. Rev. Lett. **106**, 106802 (2011).
[4] T. H. Hsieh, H. Lin, J. Liu, W. Duan, A. Bansil, and L. Fu, Nat. Commun. **3**, 982 (2012).
[5] Y. Tanaka, Z. Ren, T. Sato, K. Nakayama, S. Souma, T. Takahashi, K. Segawa, and Y. Ando, Nat. Phys. **8**, 800 (2012).
[6] L. Fu and C. L. Kane, Phys. Rev. Lett. **100**, 096407 (2008).
[7] E. Sajadi, T. Palomaki, Z. Fei, W. Zhao, P. Bement, C. Olsen, S. Luescher, X. Xu, J. A. Folk, and D. H. Cobden, Science **362**, 922 (2018).
[8] V. Fatemi, S. Wu, Y. Cao, L. Bretheau, Q. D. Gibson, K. Watanabe, T. Taniguchi, R. J. Cava, and P. Jarillo-Herrero, Science **362**, 926 (2018).
[9] W. A. Benalcazar, B. A. Bernevig, and T. L. Hughes, Science **357**, 61 (2017).
[10] F. Schindler, A. M. Cook, M. G. Vergniory, Z. Wang, S. S. P. Parkin, B. A. Bernevig, and T. Neupert, Sci. Adv. **4**, eaat0346 (2018).
[11] X. Wan, A. M. Turner, A. Vishwanath, and S. Y. Savrasov, Phys. Rev. B **83**, 205101 (2011).
[12] Z. Wang, Y. Sun, X. Q. Chen, C. Franchini, G. Xu, H. Weng, X. Dai, and Z. Fang, Phys. Rev. B **85**, 195320 (2012).
[13] Z. K. Liu, B. Zhou, Y. Zhang, Z. J. Wang, H. M. Weng, D. Prabhakaran, S. K. Mo, Z. X. Shen, Z. Fang, X. Dai *et al.*, Science **343**, 864 (2014).
[14] S. M. Young, S. Zaheer, J. C. Y. Teo, C. L. Kane, E. J. Mele, and A. M. Rappe, Phys. Rev. Lett. **108**, 140405 (2012).
[15] B. J. Yang and N. Nagaosa, Nat. Commun. **5**, 4898 (2014).
[16] Y. J. Jin, B. B. Zheng, X. L. Xiao, Z. J. Chen, Y. Xu, and H. Xu, Phys. Rev. Lett. **125**, 116402 (2020).
[17] S. Y. Xu, I. Belopolski, N. Alidoust, M. Neupane, G. Bian, C. Zhang, R. Sankar, G. Chang, Z. Yuan, C. C. Lee *et al.*, Science **349**, 613 (2015).
[18] B. Q. Lv, H. M. Weng, B. B. Fu, X. P. Wang, H. Miao, J. Ma, P. Richard, X. C. Huang, L. X. Zhao, G. F. Chen *et al.*, Phys. Rev. X **5**, 031013 (2015).
[19] Y. J. Jin, Y. Xu, Z. J. Chen, and H. Xu, Phys. Rev. B **105**, 035141 (2022).
[20] R. Yu, H. Weng, Z. Fang, X. Dai, and X. Hu, Phys. Rev. Lett. **115**, 036807 (2015).
[21] C. Fang, Y. Chen, H. Y. Kee, and L. Fu, Phys. Rev. B **92**, 081201 (2015).
[22] H. Weng, Y. Liang, Q. Xu, R. Yu, Z. Fang, X. Dai, and Y. Kawazoe, Phys. Rev. B **92**, 045108 (2015).
[23] Z. Fang, N. Nagaosa, K. S. Takahashi, A. Asamitsu, R. Mathieu, T. Ogasawara, H. Yamada, M. Kawasaki, Y. Tokura, and K. Terakura, Science **302**, 92 (2003).
[24] M. Udagawa and E. J. Bergholtz, Phys. Rev. Lett. **117**, 086401 (2016).
[25] N. P. Armitage, E. J. Mele, and A. Vishwanath, Rev. Mod. Phys. **90**, 015001 (2018).
[26] Z. Gao, M. Hua, H. Zhang, and X. Zhang, Phys. Rev. B **93**, 205109 (2016).
[27] O. Vafek and A. Vishwanath, Annu. Rev. Condens. Matter Phys. **5**, 83 (2014).
[28] T. Zhang, Z. Song, A. Alexandradinata, H. Weng, C. Fang, L. Lu, and Z. Fang, Phys. Rev. Lett. **120**, 016401 (2018).
[29] H. Miao, T. T. Zhang, L. Wang, D. Meyers, A. H. Said, Y. L. Wang, Y. G. Shi, H. M. Weng, Z. Fang, and M. P. M. Dean, Phys. Rev. Lett. **121**, 035302 (2018).

[30] Z.-M. Yu, Z. Zhang, G. B. Liu, W. Wu, X. P. Li, R. W. Zhang, S. A. Yang, and Y. Yao, Sci. Bull. **67**, 375 (2022).
[31] H. Nielsen and M. Ninomiya, Nucl. Phys. B **185**, 20 (1981).
[32] H. Nielsen and M. Ninomiya, Nucl. Phys. B **193**, 173 (1981).
[33] R. Wang, B. W. Xia, Z. J. Chen, B. B. Zheng, Y. J. Zhao, and H. Xu, Phys. Rev. Lett. **124**, 105303 (2020).
[34] Q. B. Liu, Y. Qian, H. H. Fu, and Z. Wang, npj Comput. Mater. **6**, 95 (2020).
[35] Z. Huang, Z. Chen, B. Zheng, and H. Xu, npj Comput. Mater. **6**, 87 (2020).
[36] J. Li, Q. Xie, S. Ullah, R. Li, H. Ma, D. Li, Y. Li, and X. Q. Chen, Phys. Rev. B **97**, 054305 (2018).
[37] T. Zhang, R. Takahashi, C. Fang, and S. Murakami, Phys. Rev. B **102**, 125148 (2020).
[38] Y. J. Jin, Z. J. Chen, X. L. Xiao, and H. Xu, Phys. Rev. B **103**, 104101 (2021).
[39] H. Li, T. Zhang, A. Said, Y. Fu, G. Fabbris, D. G. Mazzone, J. Zhang, J. Lapano, H. N. Lee, H. C. Lei *et al.*, Phys. Rev. B **103**, 184301 (2021).
[40] Q. B. Liu, Z. Wang, and H. H. Fu, Phys. Rev. B **103**, L161303 (2021).
[41] X. Cai, L. Ye, C. Qiu, M. Xiao, R. Yu, M. Ke, and Z. Liu, Light: Sci. Appl. **9**, 38 (2020).
[42] Z. J. Chen, R. Wang, B. W. Xia, B. B. Zheng, Y. J. Jin, Y. J. Zhao, and H. Xu, Phys. Rev. Lett. **126**, 185301 (2021).
[43] J. Li, L. Wang, J. Liu, R. Li, Z. Zhang, and X. Q. Chen, Phys. Rev. B **101**, 081403 (2020).
[44] S. Park, Y. Hwang, H. C. Choi, and B. J. Yang, Nat. Commun. **12**, 6781 (2021).
[45] G. Liu, Y. Jin, Z. Chen, and H. Xu, Phys. Rev. B **104**, 024304 (2021).
[46] J. Li, Q. Xie, J. Liu, R. Li, M. Liu, L. Wang, D. Li, Y. Li, and X. Q. Chen, Phys. Rev. B **101**, 024301 (2020).
[47] T. T. Zhang, H. Miao, Q. Wang, J. Q. Lin, Y. Cao, G. Fabbris, A. H. Said, X. Liu, H. C. Lei, Z. Fang *et al.*, Phys. Rev. Lett. **123**, 245302 (2019).
[48] C. Xie, H. Yuan, Y. Liu, X. Wang, and G. Zhang, Phys. Rev. B **104**, 134303 (2021).
[49] Q. B. Liu, Z. Q. Wang, and H. H. Fu, Phys. Rev. B **104**, L041405 (2021).
[50] A. Ptok, A. Kobiałka, M. Sternik, J. Łażewski, P. T. Jochym, A. M. Oleś, S. Stankov, and P. Piekarz, Phys. Rev. B **104**, 054305 (2021).
[51] H. He, C. Qiu, X. Cai, M. Xiao, M. Ke, F. Zhang, and Z. Liu, Nat. Commun. **11**, 1820 (2020).
[52] J. Wang, H. Yuan, M. Kuang, T. Yang, Z. M. Yu, Z. Zhang, and X. Wang, Phys. Rev. B **104**, L041107 (2021).
[53] F. Zhou, Z. Zhang, H. Chen, M. Kuang, T. Yang, and X. Wang, Phys. Rev. B **104**, 174108 (2021).
[54] Q. B. Liu, H. H. Fu, and R. Wu, Phys. Rev. B **104**, 045409 (2021).
[55] See Supplemental Material at http://link.aps.org/supplemental/10.1103/PhysRevB.106.054306 for the computational method, effective model analysis, and more materials, which includes Refs. [59–67].
[56] A. A. Soluyanov and D. Vanderbilt, Phys. Rev. B **83**, 235401 (2011).
[57] R. Yu, X. L. Qi, A. Bernevig, Z. Fang, and X. Dai, Phys. Rev. B **84**, 075119 (2011).
[58] D. Trinschek and M. Jansen, Z. Naturforsch. B **51**, 917 (1996).
[59] W. Kohn and L. J. Sham, Phys. Rev. **140**, A1133 (1965).
[60] G. Kresse and J. Furthmüller, Phys. Rev. B **54**, 11169 (1996).
[61] G. Kresse and J. Furthmüller, Comput. Mater. Sci. **6**, 15 (1996).
[62] J. P. Perdew, K. Burke, and M. Ernzerhof, Phys. Rev. Lett. **77**, 3865 (1996).
[63] G. Kresse and D. Joubert, Phys. Rev. B **59**, 1758 (1999).
[64] D. M. Ceperley and B. J. Alder, Phys. Rev. Lett. **45**, 566 (1980).
[65] A. Togo and I. Tanaka, Scr. Mater. **108**, 1 (2015).
[66] Q. Wu, S. Zhang, H. F. Song, M. Troyer, and A. A. Soluyanov, Comput. Phys. Commun. **224**, 405 (2018).
[67] M. P. L. Sancho, J. M. L. Sancho, and J. Rubio, J. Phys. F: Met. Phys. **14**, 1205 (1984).